JACS
JOURNAL OF THE AMERICAN CHEMICAL SOCIETY

ARTICLE

pubs.acs.org/JACS

Noble Metal-Free Hydrazine Fuel Cell Catalysts: EPOC Effect in Competing Chemical and Electrochemical Reaction Pathways

Jean Sanabria-Chinchilla,[†] Koichiro Asazawa,[‡] Tomokazu Sakamoto,[‡] Koji Yamada,[‡] Hirohisa Tanaka,[‡] and Peter Strasser*[,§]

[†]Department of Chemical and Biomolecular Engineering, University of Houston, Houston Texas 77204, United States

[‡]Frontier Technology R&D Division, Daihatsu Motor Co., Ltd., 3000 Yamanoue, Ryuo, Gamo, Shiga 520-2593, Japan

[§]The Electrochemical Energy, Catalysis, and Materials Science Laboratory, Department of Chemistry, Chemical Engineering Division, Technical University Berlin, 10623 Berlin, Germany

Supporting Information

ABSTRACT: We report the discovery of a highly active Ni−Co alloy electrocatalyst for the oxidation of hydrazine (N_2H_4) and provide evidence for competing electrochemical (faradaic) and chemical (nonfaradaic) reaction pathways. The electrochemical conversion of hydrazine on catalytic surfaces in fuel cells is of great scientific and technological interest, because it offers multiple redox states, complex reaction pathways, and significantly more favorable energy and power densities compared to hydrogen fuel. Structure−reactivity relations of a $Ni_{60}Co_{40}$ alloy electrocatalyst are presented with a 6-fold increase in catalytic N_2H_4 oxidation activity over today's benchmark catalysts. We further study the mechanistic pathways of the catalytic N_2H_4 conversion as function of the applied electrode potential using differentially pumped electrochemical mass spectrometry (DEMS). At positive overpotentials, N_2H_4 is electrooxidized into nitrogen consuming hydroxide ions, which is the fuel cell-relevant faradaic reaction pathway. In parallel, N_2H_4 decomposes chemically into molecular nitrogen and hydrogen over a broad range of electrode potentials. The electroless chemical decomposition rate was controlled by the electrode potential, suggesting a rare example of a liquid-phase electrochemical promotion effect of a chemical catalytic reaction ("EPOC"). The coexisting electrocatalytic (faradaic) and heterogeneous catalytic (electroless, nonfaradaic) reaction pathways have important implications for the efficiency of hydrazine fuel cells.

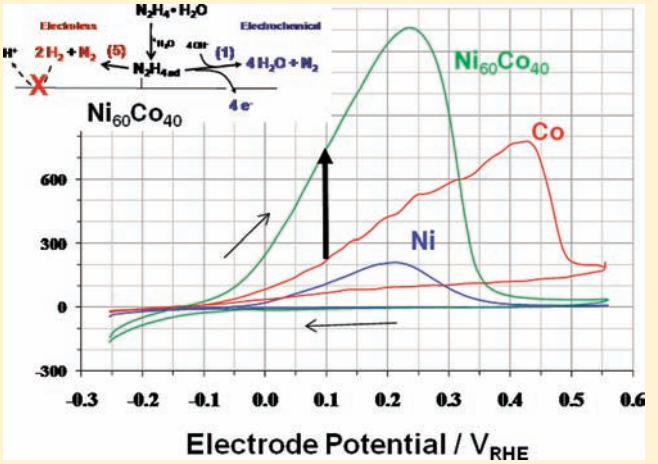

1. INTRODUCTION

Electrochemical catalysis and heterogeneous chemical catalysis share many elementary principles, such as surface adsorption of reactants, activated surface reactions of intermediates via transition states, or surface desorption forming reaction products. They sharply differ, however, in the nature of their redox electron transfer across the catalytic interface. Given the absence of charged species, chemical catalysis uses pressure and temperature as the two key control parameters to affect the Gibbs free energy of reaction and the associated Gibbs free energy of activation, that is, the energy of the activated complex in the transition state. Owing to the presence of charges species and electrons, electrochemical catalysis leverages the electrode potential as well in order to affect Gibbs free energies of reaction and activation. From this, one would hypothesize that, if electrochemical and chemical reactions share similar intermediates or transition states, electrode potential could affect and possibly promote rates of nonfaradaic chemical catalysis, as well. This is demonstrated here for the electrooxidation of hydrazine on novel highly active non-noble alloy electrocatalysts.

Hydrazine (N_2H_4) is a high-energy fuel molecule, the catalysis of which has been studied as early as 1912.[1,2] The long interest in developing high-power density direct hydrazine−air fuel cells[3] is based on their following unique advantages: (i) the theoretical standard equilibrium hydrazine cell potential of +1.56 V is superior to those of other liquid or H_2−air fuel cells. The electrode reactions read

$$\text{Anode}: \ N_2H_4 + 4OH^- \leftrightarrows N_2 + 4H_2O + 4e^- \qquad E^\circ = -0.33\ \text{V/RHE} \tag{1}$$

$$\text{Cathode}: \ O_2 + 2H_2O + 4e^- \leftrightarrows 4OH^- \qquad E^\circ = +1.23\ \text{V/RHE} \tag{2}$$

$$\text{Cell Reaction}: \ N_2H_4 + O_2 \leftrightarrows N_2 + 2H_2O \qquad E^\circ = +1.56\ \text{V/RHE} \tag{3}$$

Received: December 11, 2010
Published: March 22, 2011

   dx.doi.org/10.1021/ja111160r | J. Am. Chem. Soc. 2011, 133, 5425–5431

(ii) the products of hydrazine oxidation (nitrogen and water) are neither harmful nor carbon-containing, (iii) the cell operates at near-ambient temperatures (40−80 °C), (iv) the hydrazine fuel cell offers superior energy and power densities compared to hydrogen fuel cell (5400 W h L^{-1}) making it ideally suited for automotive applications. In a previous report, we have demonstrated a detoxification technique which safely fixed hydrazine to the carbonyl groups in the polymer and released hydrazine by means of a solvent at the time of power generation.[4]

The hydrazine standard electrode potential is more negative than that of the hydrogen evolution reaction (HER):

$$2H_2O + 4e^- \leftrightarrows 2OH^- + H_2 \quad E^o = 0.00\ V/RHE \qquad (4)$$

Therefore, depending on the kinetics of the hydrogen half cell system on the selected catalyst material, a complex mixed potential based on the concomitant electrooxidation of aqueous N_2H_4 (reaction 1) and the HER may occur.[5,6] On noble metals, such as Pt, an electroless (nonfaradaic) purely chemical catalytic decomposition pathway was reported:[7]

$$N_2H_4 \rightarrow N_2 + 2H_2 \qquad (5)$$

$$3N_2H_4 \rightarrow 2N_2 + 4NH_3 \qquad (6)$$

The electrooxidation of hydrazine in alkaline media was investigated extensively at platinum,[8−12] palladium,[13−15] gold,[12,16] mercury,[11,16−18] and silver[19] electrodes. Yi et al.[19] studied the alkaline hydrazine electrooxidation on Ti-supported Ag−Ni nanoparticles and reported high catalytic activities for a $Ag_{86}Ni_{14}$ alloy. Recently, Ye et al.[14] studied Ni−Pd alloy nanoparticles and found improved hydrazine oxidation activities. Rosca and Koper[20] presented a comparative Tafel-slope study of hydrazine electrooxidation on Pt in alkaline and acidic solutions. Using online mass spectrometry, they confirmed earlier reports[21] that molecular nitrogen is the major reaction product. Early on, a nonfaradaic catalytic breaking of the N−H bond on Pt was hypothesized[15,22] yet never confirmed due to the immediate electrooxidation of surface atomic hydrogen. More recent reports addressed the design of direct hydrazine polymer electrolyte membrane fuel cell (PEMFCs),[4,7,23−28] comparing different anode materials[7] and anion-exchange membranes.[29] Employing non-noble anode monometallic electrocatalysts, a distinct sensitivity of the cell performance on the alkaline concentration was detected.[27] Despite these recent studies on non-noble electrocatalysts, a more detailed mechanistic understanding of the relevant mechanistic reaction pathways is still missing. While pure Co and Ni catalysts show catalytic activities comparable to that of Pt[30] and are the anode catalysts of choice in alkaline media, catalytic activity benefits of bimetallic noble metal-free alloy catalysts have never been investigated for the hydrazine electrooxidation.

Here, we investigate the electrocatalytic oxidation of hydrazine on non-noble bimetallic electrocatalysts, benchmarking their catalytic activity against state-of-the-art Co and Ni monometallic catalysts. We report a new bimetallic catalyst system with unprecedented catalytic hydrazine oxidation activity. Using in situ differentially pumped electrochemical mass spectrometry (DEMS) we report evidence for a mechanistic competition of two parallel catalytic hydrazine conversion pathways, one purely chemical electroless (reaction 5) and the other electrochemical faradaic (reaction 1). We find that the rate of the electroless chemical catalysis shows a dependence on the applied external electrode potential, a rare example of an electric field-based influence on heterogeneous catalytic reactions (EPOC effect[31−38]) in low-temperature liquid electrolyte electrochemistry. We hypothesize that shared surface transition states and/or reactive intermediates of the hydrazine molecule is the origin for the EPOC effect.

2. EXPERIMENTAL METHODS

2.1. Catalyst Synthesis. Carbon-supported Ni, Co, and NiM (M = Co, Cu, Zn, Fe, Ag, Mn, Zr) and CoZn bimetallic catalyst libraries with stoichiometries from (90:10) to (20:80) were prepared by an impregnation/freeze-drying procedure followed by thermal annealing. Preparation started with impregnation and sonication of high-surface-area carbon (HSC) (Ketjenblack EC 300J, Akzo Nobel) with aqueous metal-salt solutions.[39] Solutions were either commercially available, e.g., $ZrO(NO_3)_2$ in 35 wt % nitric acid or made from precursor compounds [e.g., $Ni(NO_3)_2 \cdot 6H_2O$ or $Fe(NO_3)_3 \cdot 9H_2O$] dissolved in deionized (DI) water (>18.2 MΩ cm) Milli-Q gradient system, Millipore Inc.). Ni and Mn precursors were obtained from Alfa Aesar; all other metal precursors and solutions were obtained from Sigma-Aldrich, Inc. A robotic liquid dispenser (Tecan Systems, United States) was utilized to pipet the desired amount of metal solution onto the carbon powder substrate for metal impregnation. Once these slurries were sonicated, the impregnated catalysts were then frozen in liquid N_2 and subsequently freeze-dried under a moderate vacuum (0.055 mbar). All catalysts were prepared in ∼10 mL quartz vials. Reduction of metal precursors to the zerovalent state on the carbon support was thermally driven under a reductive H_2 atmosphere (6% H_2, balance Ar, Matheson Tri·Gas) at 250 °C for 2.5 h using a Lindberg/blue tube furnace. Final thermal annealing was performed immediately after the reduction step at 800 °C for 8 h. Each bimetallic library was designed to contain eight catalyst samples. The atomic composition (as at %) of each sample was varied in 10 at % increments from (90:10) to (20:80). All catalyst samples contained 30 wt % total metal on HSC support.

2.2. Parallel Electrochemical High Throughput Screening of Electrocatalysts. A (4 × 4)16-channel electrochemical electrode array for parallel testing of alloy electrocatalysts was utilized in this study. This array was previously described in detail.[39] The array consisted of mirror-polished glassy carbon (GC) electrodes (see Figure S1), onto which the different catalyst powders were applied as catalyst powder thin film based on the procedure originally reported by Schmidt et al.[40,41]. Each of these working electrodes was *i*) in contact with independent samples of the testing solution, and *ii*) independently controlled by a potentiostat.

Due to the use of strong alkaline media, a Zn/ZnO quasi reference electrode was utilized instead of the conventional Ag/AgCl reference electrode. The reference electrode comprised a Zn wire immersed in 1.0 M KOH solution, and it was calibrated against a hydrogen reference electrode (Hydroflex RE, Gaskatel GmbH, Germany). A Pt wire served as counter electrode. All potentials presented and discussed here are reported against a reference hydrogen electrode (RHE) at pH 14.

Catalyst inks were prepared in a manner nearly identical to that previously published.[42−44] In short, 10 mg of the desired catalyst was combined with 7.5 mL of DI water, 1.5 mL of isopropanol, 0.460 mL of THF, and 40.0 μL of a 5 wt % anionic ionomer solution (Daihatsu Motor Co.). The ink was then sonicated during 15 min. After sonication, 39.2 μL of the ink was applied onto the GC electrode, resulting in a loading of 15 $\mu g_{total\ metal}/cm^2$. The entire array was then left to dry for at least 1 h.

For each of the eight catalyst samples of each library, two ink applications were randomly applied in two different GC electrodes. One catalyst film was immersed in 1.0 M KOH solution [50% w/v aq sol., Alfa Aesar], whereas the other one was immersed in 0.1 M hydrazine hydrate/1.0 M KOH solution [60% v/v hydrazine hydrate solution,

Ootsuka Chemistry Inc., Japan]. Each of the 16 chambers in the array was then bubbled with N_2 gas (UHP, Matheson Tri·Gas) to remove any unwanted gases from the solutions. After 15 min, the gas was switched to a "blanketing" flow. The catalyst films were then cycled 1000 times between −0.25 V and +0.10 V (vs RHE) at 20 mV/s (durability test) and then three consecutive linear sweep voltammograms (LSV) were run from −0.25 V to +0.10 V (vs RHE) at 5 mV/s. From these LSV runs, the mean mass activity value for each catalyst sample was calculated by obtaining the maximum current at +0.10 V. Mass activity values were expressed as metal-based mass current ($A/g_{\text{total metal}}$).

2.4. Rotating Disk Electrode (RDE) Measurements. RDE activity measurements were performed in a three-electrode configuration on a 10 mm glassy carbon (GC) disk electrode in 0.1 M HH/1.0 M KOH electrolyte. Due to the strong alkaline media utilized in this study, a custom-made temperature-controlled Teflon electrochemical cell was built for the RDE testing. The ink and electrode thin-film preparation procedures as well as the measurement protocols of the RDE testing were identical to those for parallel array testing with the following exceptions: (i) The temperature was increased from 25 to 60 °C; (ii) speed rotation was set at 900 rpm. A BiStat potentiostat (BioLogic Science Instrument) was utilized in the RDE testing. Speed rotation was set through a rotating electrode spin control (Pine Research Instrumentation). A Pt wire was used as counter electrode and a Zn/ZnO reference electrode (E° = −0.432 V/RHE, −1.26 V/$NHE_{pH=0}$). All potentials are reported with respect to a reversible RHE. Electrochemical characterization of the catalyst film was performed following the same experimental protocol used with the combinatorial array.

2.5. Catalyst Characterization by XRD. Laboratory-source XRD (Siemens D5000 $\theta/2\theta$ diffractometer) was used to characterize the electrocatalysts structurally. The diffractrometer is equipped with a Braun position sensitive detector (PSD) with an angular range of 8°. The Cu Kα source operates at a potential of 35 kV and current of 30 mA. Diffraction angles (2θ) ranged from 20° to 70°, scanned with step size of 0.02° per step and holding time of 10−30 s per step. Advanced X-ray solution (X-ray Commander, Bruker AXS) software was used to control the diffractometer from a desktop computer. The XRD sample holder was a custom-made 3 cm × 3 cm plexiglass with a 1 cm width × 2 cm length × 1 mm depth well in the center that holds the powder catalyst samples. The catalyst powder was poured into the well and carefully flattened to form a smooth surface, flush with the surface of the plexiglass. XRD patterns were analyzed by JADE 8.1 software (MDI): Peak profiles of individual reflections were obtained by a nonlinear least-squares fit of the Cu $K\alpha_2$ corrected data.

2.6. Differentially Pumped Electrochemical Mass Spectrometry (DEMS). DEMS experiments were performed using a differentially pumped ThermoStar GSD 301 Pfeiffer gas analyzer (Pfeiffer Vacuum, United States) with a liquid-to-gas interface containing a Silastic tubing (Dow Corning, United States) for diffusion of gaseous and volatile species into the differentlially pumped area of the spectrometer. During measurements, the polymeric probe interface was placed inside the electrolyte of the electrochemical cell next to the RDE catalyst interface (about 1−2 cm distance). Instead of N_2 gas for blanketing, Ar gas (UHP, Matheson Tri·Gas) was used when m/z = 28 was monitored.

3. RESULTS AND DISCUSSION

3.1. Hydrazine Electrooxidation on Ni and Co Electrodes. Figure 1 compares the initial electrocatalytic behavior of pure Ni (blue) and pure Co (red) nanoparticles (a) in absence and (b) in presence of hydrazine hydrate, $N_2H_4 \cdot H_2O$ (HH). Also included in Figure.1 is a voltammetry of a Ni−Co alloy, which will be discussed later. The voltammetric features in Figure 1a represent the electrode potential-dependent surface chemistries of each catalytic interfaces. The anodic voltammetric peaks on the positive-going

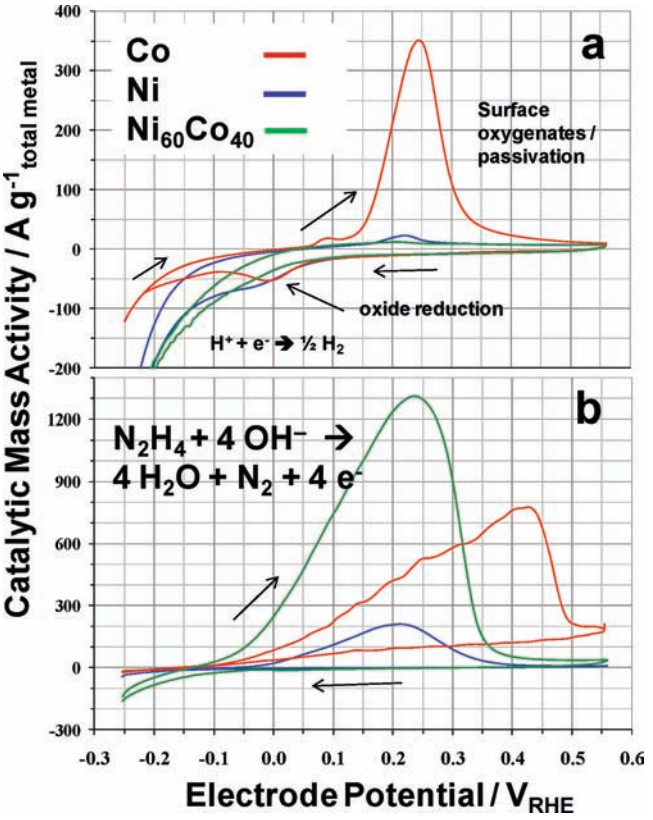

Figure 1. Cyclic voltammograms of Ni, Co, and a novel $Ni_{60}Co_{40}$ electrocatalysts in (a) argon-saturated 1.0 M KOH solution and (b) in 0.1 M hydrazine hydrate $N_2H_4 \cdot H_2O$ (HH)/1.0 M KOH solution. Plotted is the metal mass-based catalytic current. Conditions: RDE, 60 °C, 900 rpm, 20 mV/s.

potential scans of Ni (+0.23 V, weak) and Co (+0.08 V, weak, and +0.25 V, strong) in Figure 1a suggest the formation of higher-valent Co and Ni surface oxygenates on the basis of the interaction of OH^- with the metal surface according to

$$M + OH^- \leftrightarrows M - OH + e^- \quad (7)$$

$$M + 2OH^- \leftrightarrows M(OH)_2 + 2e^- \quad (8)$$

where M represents a surface metal atom. The passivating effect of the surface metal hydroxide layers for the hydrazine electrooxidation becomes evident when comparing voltammograms a and b in Figure 1. The electrocatalytic HH oxidation on Ni (Figure 1b) first rises, then rapidly drops upon Ni passivation above +0.23 V. On a Co surface, the HH electrooxidation drops past +0.43 V, most likely due to the delayed passivating effect of Co oxygenates based on their better solubility,[45] which is consistent with the larger Co passivation charge. At potentials above 0.5 V in Figure 1b, HH electrooxidation is low on both surfaces, with Co showing some residual activity.

After reversing the potential scan at +0.56 V (Figure 1b), no hydrazine oxidation was observed during the cathodic scan (cathodic arrow) evidencing the irreversible nature of the metal passivation.[24] Active Co and Ni interfaces can be recovered by scanning below 0.0 V/RHE as shown by the reduction peaks in Figure 1a. Upon repeated passivation−reactivation cycles between −0.25 V to +0.56 V, Ni catalysts eventually exhibited superior HH electrooxidation activities in agreement with previous reports.[30]

dx.doi.org/10.1021/ja111160r |J. Am. Chem. Soc. 2011, 133, 5425–5431

3.2. Electrocatalytic Hydrazine Oxidation on Non-Noble Alloys. Eight different bimetallic catalyst libraries (Ni−Co, Ni−Cu, Ni−Zn, Ni−Fe, Ni−Ag, Ni−Mn, Ni−Zr, and Co−Zn) were prepared and tested for hydrazine electrooxidation and benchmarked against pure Co and Ni (Table S1, Supporting Information [SI]). Each library included eight different binary compositions at a 10 at % interval (Table S2, SI). A stationary electrochemical electrode array[39,46−49] (Figure S1, SI) was used to test the catalytic HH oxidation activity and stability of a total of 64 different catalysts.

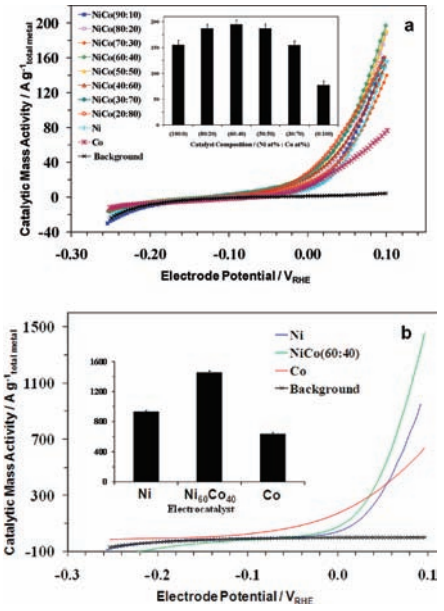

Figure 2. (a) Parallel evaluation of hydrazine electrooxidation activities of Ni−Co bimetallic catalysts on a stationary electrode array compared to Co and Ni benchmarks. Shown are anodic voltammetric sweeps after 1000 cycles between −0.25 V and +0.10 V. The background was measured in HH-free electrolyte. 0.1 M HH/1.0 M KOH, 25 °C, 5 mV/s. Inset: Mass activities at +0.10 V. (b) RDE voltammetry of the novel $Ni_{60}Co_{40}$ catalyst confirmed the screening trends from (a); all conditions as in (a). Insets a and b: RDE catalytic mass activities in $A/g_{total\ metal}$ at +0.10 V.

Table S1 reveals that Ni−Co bimetallic alloys are more active than Ni and Co and superior to all other bimetallic systems. In particular, Figure 2a reveals that Co exhibited a low hydrazine oxidation onset potential, while Ni is more active than Co at +0.10 V after potential cycling in agreement with earlier reports.[50] A novel bimetallic $Ni_{60}Co_{40}$ composition showed unprecedented HH electrooxidation activity. RDE measurements of scaled-up catalysts (Figure 2b) confirmed the screening trends for Ni, Co, and the novel $Ni_{60}Co_{40}$ composition. Our RDE data suggest a nearly 100% increase in HH electrooxidation activity on the bimetallic catalyst compared to that of pure Co.

To obtain insight in the atomic structure of the highly active hydrazine oxidation catalyst, we performed bulk structural X-ray scattering analysis (Figure 3). All Ni−Co bimetallics were face-centered cubic (space group $Fm\bar{3}m$) substitutional solid solutions (disordered alloys). Table S2 (SI) summarizes ICP-OES-derived compositions of the most active catalysts, showing that they are in excellent agreement with their nominal library composition.

The voltammetric features of the $Ni_{60}Co_{40}$ catalyst (green) in Figure 1a suggest reduced surface passivation on the anodic scan. The HH oxidation activity (Figure 1b) is about 6x higher than that of Ni and about 2× higher than that of Co. Similar to Ni, the HH oxidation activity of the alloy peaks at +0.23 V and drops to near zero values past 0.5 V. Noteworthy, the HH oxidation onset potential of −0.15 V of the novel $Ni_{60}Co_{40}$ catalyst is significantly shifted lower electrode potentials compared to pure Co and Ni offering high cell efficiencies at low current densities.

3.3. Mechanistic Pathways and Electrochemical Promotion of Catalysis (EPOC Effect). *The Hydrogen Oxidation Reaction on Ni−Co Alloys.* To arrive at a conclusive mechanistic understanding of major reaction pathways, we first needed to investigate the hydrogen redox reactivity (eq 4) of our novel

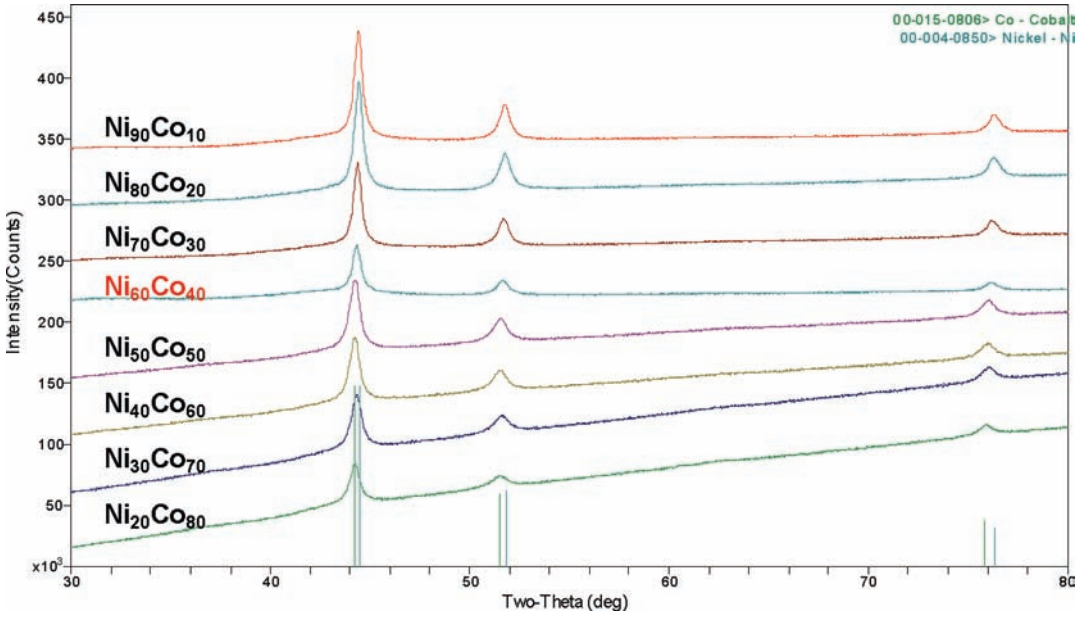

Figure 3. Powder X-ray diffraction profiles of the most active set of Ni−Co bimetallic electrocatalysts. The Ni−Co materials exhibit solid solutions. $Ni_{60}Co_{40}$ is the most active HH oxidation catalyst. Stick pattern show pure Co (cyan) and pure Ni(green).

dx.doi.org/10.1021/ja111160r |*J. Am. Chem. Soc.* 2011, 133, 5425–5431

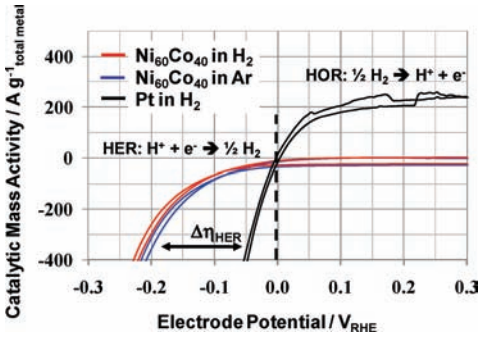

Figure 4. Hydrogen oxidation reaction (HOR) and hydrogen evolution reaction (HER) activity of the $Ni_{60}Co_{40}$ bimetallic catalyst in H_2-saturated (red) and Ar-saturated (blue) 1 M KOH electrolyte. HER and HOR on a Pt in H_2-saturated KOH is shown for comparison (black). $Ni_{60}Co_{40}$ shows negligible activity for HOR and a significant HER overpotential $\Delta\eta_{HER}$ compared to Pt. conditions: 25 °C, scan rate 50 mV/s.

$Ni_{60}Co_{40}$ catalyst, that is, the electrode potential-dependent rate of the hydrogen evolution reaction (HER) and the hydrogen oxidation reaction (HOR). Figure 4 reports the HOR and HER behavior of the $Ni_{60}Co_{40}$ catalyst in H_2-saturated electrolyte (red) compared to a Pt catalyst (black). While Pt shows a diffusion-limited HOR reactivity beyond +0.05 V and highly active HER,[51] $Ni_{60}Co_{40}$ exhibited no detectable activity for the HOR and a very large overpotential for the HER (blue in Figure 4). We conclude that the $Ni_{60}Co_{40}$ alloy has a very low tendency to adsorb atomic hydrogen,[52,53] the key intermediate in the HOR and HER reaction.

The absence of any HOR activity on the $Ni_{60}Co_{40}$ was important, because it enabled us to *directly* detect and quantify the nonfaradaic HH decomposition (reaction 5) by measuring the rate of molecular hydrogen formation. On noble metal catalysts, such as Pt or Pd, which readily oxidize molecular hydrogen, this would not be possible.

Differentially Pumped Electrochemical Mass Spectrometry. Insight into relevant mechanistic reaction pathways of the HH electrooxidation on $Ni_{60}Co_{40}$ was achieved by differentially pumped electrochemical mass spectrometry (DEMS).[54,55] DEMS is a powerful analytical technique which probes in situ volatile chemical products formed at electrified catalytic interfaces. Graphs a and b of Figure 5 show the temporal evolution of the ion mass currents for H_2 and N_2, respectively, at the electrode potential of zero faradaic current (open circuit potential, OCP) (red lines) and at an electrode potential of +0.10 V/RHE (blue lines). At OCP, formation of molecular H_2 in the presence of hydrazine evidenced the *electroless, nonfaradaic chemical* HH decomposition according to reaction 5. After an initial rapid increase, the rate of hydrogen formation by the nonfaradaic HH decomposition gradually decreased before it approached a near-stationary plateau.

At an electrode potential of +0.10 V, a faradaic anodic current associated with the electrocatalytic oxidation of HH to nitrogen and protons according to reaction 1 is observed. Now, a sustained *increased* molecular H_2 production rate suggested an enhanced electroless (nonfaradaic) catalytic HH decomposition.[38] The applied electrochemical potential and the associated faradaic current appear to promote the purely chemical catalytic HH decomposition. Based on reaction eqs 1 and 5, the rate of nitrogen formation should increase at positive electrode

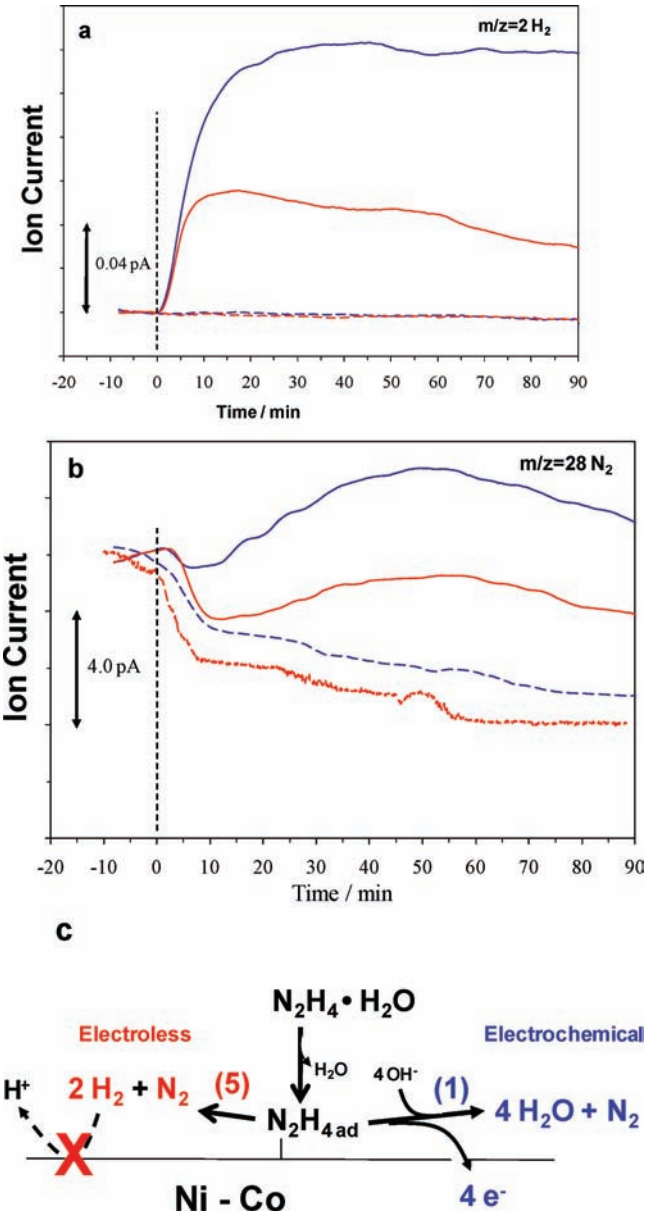

Figure 5. Evolution of (a) hydrogen ($m/z = 2$) and (b) nitrogen ($m/z = 28$) ions mass currents at open circuit potentials (red), that is, at zero faradaic current, and at +0.10 V/RHE (blue) in the presence (solid) and absence (dashed) of hydrazine (HH) using DEMS. $t = 0$ marks the instant when the catalyst was placed in contact with the solution at the specified potential. (c) Proposed competing chemical (red, reaction 5) and electrochemical (blue, reaction 1) HH decomposition pathways. The presence of the faradaic current was found to enhance the rate of the chemical nonfaradaic pathway (EPOC effect).

potentials, because the N_2 formation according to eqs 1 and 5 will add up. In fact, this behavior is observed in the temporal N_2 ion current ($m/z = 28$) profile at OCP (solid red curve) and at +0.1 V/RHE (solid blue curve) in Figure 5b. We want to point out that the values of the absolute ion currents sensitively depend on the pressure and ionization conditions inside the instrument and hence do not allow for a direct quantitative comparison between species. We also note that the ion current baseline of $m/z = 28$ in Figure 5b displayed a high sensitivity to hydrodynamic perturbations; the insertion of the working electrode into the

dx.doi.org/10.1021/ja111160r | J. Am. Chem. Soc. 2011, 133, 5425–5431

electrolyte at $t = 0$ resulted in reproducible transient decreases in the current baselines associated with changes in the nitrogen pressure inside the mass spec ionization chamber.

The EPOC effect. The enhancement of a nonfaradaic catalytic surface reaction in the presence of an interfacial potential associated with an electrochemical faradaic current is referred to as an "electrochemical promotion of chemical catalysis" effect (EPOC effect).[31−38] The EPOC effect was first described by Vayenas and his group[31] in a heterogeneous catalytic reaction between gaseous adsorbates on metal surfaces supported on solid electrolytes. The catalytic metals were typically deposited as porous films onto solid ion conducting electrolytes,[31,32,56] such as O^{2-} conducting yttrium-stabilized zirconium dioxide (YSZ).[57] Electrochemically induced catalytic rate increases up to a factor of 200[34] were reported. The EPOC effect is perceived as a phenomenon linking electrocatalysis and heterogeneous catalysis at the molecular level. Earlier mechanistic hypothesis for the EPOC effect on solid electrolytes repeatedly cited the role of modifications of the local work function[32−34] of the metal surface by spilled-over oxygen anions and their effect on the chemisorption strengths of metal surface adsorbates. While the presence of spilled over charged species on the catalytic metals has been confirmed by various groups, a very recent review of the EPOC effect[38] has critically revisited the alleged controlling mechanistic role of the surface work function in the light of modern surface science. The review concluded that the surface work function possibly plays a more minor role in our current understanding of surface catalysis than previously thought. On the other hand, more recent concepts and descriptors in heterogeneous catalysis, such as the d-band center position relative to the Fermi level energy, have gained importance to explain trends and modifications in catalytic reactivity.[58] A rare case of an EPOC effect in a liquid electrolyte included the chemical and electrochemical reaction of mixtures of hydrogen and oxygen on Pt catalysts in alkaline solutions.[34,35] Similarly to solid electrolytes, the modification of the local work function and surface binding strengths were cited as the origin of the EPOC effect in liquid electrolytes.[34] However, no clear physical explanation was provided whether or how charged surface species can influence surface properties of the metal electrode.

To explain the observed EPOC effect in the present case of the HH oxidation reaction we hypothesize the existence of a hydrazine surface adsorbate, which serves as a reactive intermediate for both the faradaic (reaction 1) and the nonfaradaic (reaction 5) pathway. This hypothesis would imply that the two reactions pathways originate on structurally similar surface sites or defects on the Ni−Co electrode and could share a structurally similar transition state. These sites break N−H bonds and subsequently adsorb hydrazine molecules, such that they can further react either along the faradaic or the nonfaradaic pathway. At electrode potentials positive of the OCP, the local work function of the catalytic surface increases relative to that at OCP; this lowers the Gibbs free energy of protons, electrons and of the transition state and foremost drives the electrocatalytic oxidative pathway.[59] A shared or at least structurally similar transition state of the two pathways would now also result in a reaction rate increase of the nonfaradaic chemical HH decomposition and hence could account for the observed EPOC effect.

Practical implications for hydrazine−air fuel cells employing the novel Ni−Co anode catalysts include parasitic fuel loss at open-circuit (rest) conditions as well as reduced fuel efficiency under operating conditions, despite the expected significant improvement in overall cell output power.

4. CONCLUSIONS

We have developed a novel non-noble $Ni_{60}Co_{40}$ single-phase disordered alloy catalyst with unparalleled electrocatalytic activity for the HH electrooxidation (reaction 1) in potential ranges of relevance to direct alkaline hydrazine fuel cell anodes. Deployment of this new catalyst in direct hydrazine fuel cells would result in significant improvements in terms of output power of these fuel cell devices.

A mechanistic study of the HH oxidation on the novel non-noble electrocatalyst revealed the presence of parallel reaction pathways. In particular, combined cyclic voltammetry and DEMS studies evidenced the existence of two competing HH reaction pathways. One pathway is an electroless, purely chemical catalytic decomposition of HH into molecular hydrogen and nitrogen (reaction 5). The other is the electrocatalytic conversion of HH into nitrogen and water. The fact that the Ni−Co alloy catalyst does not electrooxidize molecular hydrogen enabled a direct observation of the nonfaradaic decomposition pathways of hydrazine.

Our DEMS study revealed that the rate of the nonfaradaic, chemical pathway increased in the presence of an anodic faradaic (electrochemical) HH oxidation current. This suggested an electrochemical promotion of a chemical catalytic reaction on a metal electrode interfacing with an electrolyte (EPOC effect). Typically, EPOC effects were observed at solid electrolyte/metal interfaces and mostly for chemical reactions involving oxygen[31,56,57,60] at temperatures above 300 °C. The generally accepted origin of the EPOC effect on metal electrodes supported on solid oxide electrolytes lies in the spillover of negatively charges oxide species onto the metal catalyst affecting the local work function and local reactivity. We hypothesize that the mechanistic origin of the current low-temperature EPOC effect in a liquid electrolyte lies in shared or structurally similar activated transition states and/or adsorbed surface intermediates of hydrazine oxidation and decomposition. As a result of that, promotion of the electrochemical oxidative pathway by positive electrode potentials also enhances the rate of the chemical hydrazine decomposition. This type of EPOC effect would be generally relevant where reactants of electrochemical half cells exhibit parallel chemical decomposition pathways, such as duel path mechanism often found in the electrocatalytic oxidation of small organic compounds like formic acid. Here, the electrochemical oxidation is believed to proceed in parallel with the nonfaradaic chemical decomposition of the reactant to surface bound carbon monoxide, CO.[61−66]

The coexisting nonfaradaic electrooxidation pathways of hydrazine represent a serious challenge to the fuel-efficiency of direct hydrazine fuel cells anodes, as fuel is constantly consumed and decomposes in hydrogen and nitrogen, even under idle OCP conditions.

■ ASSOCIATED CONTENT

Supporting Information. This material is available free of charge via the Internet at http://pubs.acs.org.

■ AUTHOR INFORMATION

Corresponding Author
pstrasser@tu-berlin.de

■ ACKNOWLEDGMENT

This work was supported by the Department of Energy, Office of Basic Energy Sciences, under a subcontract with Stanford Accelerator Laboratory (SLAC). P.S. acknowledges financial support by the Center of excellence (Exzellenzcluster) in catalysis ("UNICAT") funded by the German National Science Foundation (DFG) and managed by the Technical University Berlin.

■ REFERENCES

(1) Schmidt, E. W. *Hydrazine and its derivatives: preparation, properties, applications*; John Wiley & Sons: New York, 1984.
(2) Rothgery, E. F. In *Kirk-Othmer Encyclopedia of Chemical Technology*; John Wiley & Sons: New York, 2004; Vol. 13, pp 562−607.
(3) Serov, A.; Kwak, C. *Appl. Catal., B* **2010**, *98*, 1–9.
(4) Asazawa, K.; Yamada, K.; Tanaka, H.; Oka, A.; Taniguchi, M.; Kobayashi, T. *Angew. Chem., Int. Ed.* **2007**, *46*, 8024.
(5) Susbielles, G.; Bloch, O. *C. R. Acad. Sci.* **1962**, *255*, 685–687.
(6) Szpak, S.; Stonehart, P.; Katan, T. *Electrochim. Acta* **1965**, *10*, 563–583.
(7) Yamada, K.; Yasuda, K.; Tanaka, H.; Miyazaki, Y.; Kobayashi, T. *J. Power Sources* **2003**, *122*, 132–137.
(8) Petek, M.; Bruckenstein, S. *J. Electroanal. Chem.* **1973**, *47*, 329–333.
(9) Kodera, T.; Honda, M.; Kita, H. *Electrochim. Acta* **1985**, *30*, 669–675.
(10) Burke, L. D.; O'Dwyer, K. J. *Electrochim. Acta* **1989**, *34*, 1659–1664.
(11) Harrison, J. A.; Khan, Z. A. *J. Electroanal. Chem.* **1970**, *26*, 1–11.
(12) Conway, B. E.; Marincic, N.; Gilroy, D.; Rudd, E. *J. Electrochem. Soc.* **1966**, *113*, 1144–1158.
(13) Korovin, N. V.; Yanchuk, B. N. *Electrochim. Acta* **1970**, *15*, 569–580.
(14) Ye, L. Q.; Li, Z. P.; Qin, H. Y.; Zhu, J. K.; Liu, B. H. *J. Power Sources* **2011**, *196*, 956–961.
(15) Fukumoto, Y.; Matsunaga, T.; Hayashi, T. *Electrochim. Acta* **1981**, *26*, 631–636.
(16) Kořínek, K.; Koryta, J.; Musilová, M. *J. Electroanal. Chem.* **1969**, *21*, 319–327.
(17) Karp, S.; Meites, L. *J. Am. Chem. Soc.* **1969**, *84*, 906–912.
(18) Eisner, U.; Zemer, Y. *J. Electroanal. Chem.* **1972**, *34*, 81–89.
(19) Yi, Q.; Li, L.; Yu, W.; Liu, X.; Zhou, Z.; Nie, H. *Rare Met.* **2010**, *29*, 26.
(20) Rosca, V.; Koper, M. T. M. *Electrochim. Acta* **2008**, *53*, 5199–5205.
(21) Perek, M.; Bruckenstein, S. *J. Electroanal. Chem.* **1973**, *47*, 329.
(22) Kodera, T.; Honda, M.; Kita, H. *Electrochim. Acta* **1985**, *30*, 669.
(23) Karami, P. E.; Jafarloo, R.; Dorraji, P. S. *Electrochim. Acta* **2009**, *54*, 5721–5726.
(24) Asazawa, K.; Yamada, K.; Tanaka, H.; Taniguchi, M.; Oguro, K. *J. Power Sources* **2009**, *191*, 362–365.
(25) Dantas, L. M. F.; dos Reis, A. P.; Tanaka, S. M. C. N.; Zagal, J. H.; Chen, Y.-Y.; Tanaka, A. A. *J. Braz. Chem. Soc.* **2008**, *19*, 720–726.
(26) Yamada, K.; Asazawa, K.; Yasuda, K.; Ioroi, T.; Tanaka, H.; Miyazaki, Y.; Kobayashi, T. *J. Power Sources* **2003**, *115*, 236–242.
(27) Yin, W. X.; Li, Z. P.; Zhu, J. K.; Qin, H. Y. *J. Power Sources* **2008**, *182*, 520–523.
(28) Shao, J. L.; Hai, Y. Q.; Li, Q. Y.; Bin, H. L.; Zhou, P. L. *J. Power Sources* **2010**, *195*, 4135–4138.
(29) Yamada, K.; Yasuda, K.; Fujiwara, N.; Siroma, Z.; Tanaka, H.; Miyazaki, Y.; Kobayashi, T. *Electrochem. Commun.* **2003**, *5*, 892–896.
(30) Asazawa, K.; Yamada, K.; Tanaka, H.; Taniguchi, M.; Oguro, K. *J. Power Sources* **2009**, *191*, 362–365.
(31) Vayenas, C. G.; Bebelis, S.; Neophytides, S. *J. Phys. Chem.* **1988**, *92*, 5083–5085.
(32) Vayenas, C. G.; Bebelis, S.; Ladas, S. *Nature* **1990**, *343*, 625.
(33) Ladas, S.; Kennou, S.; Bebelis, S.; Vayenas, C. G. *J. Phys. Chem.* **1993**, *97*, 8845–8848.
(34) Neophytides, S. G.; Tsiplakides, D.; Stonehart, P.; Jaksic, M. M.; Vayenas, C. G. *Nature* **1994**, *370*, 45.
(35) Neophytides, S. G.; Tsiplakides, D.; Stonehart, P.; Jaksic, M.; Vayenas, C. G. *J. Phys. Chem.* **1996**, *100*, 14803–14814.
(36) Marwood, M.; Vayenas, C. G. *J. Catal.* **1998**, *178*, 429–440.
(37) Vayenas, C. G.; Bebelis, S.; Pliangos, C.; Brosda, S.; Tsiplakides, D. *Electrochemical Activation of Catalysis: Electrochemical Promotion and Metal−Support Interactions*; Kluwer Academic/Plenum Publishers: Dordrecht, Netherlands, 2001.
(38) Imbihl, R. *Prog. Surf. Sci.* **2010**, *85*, 241–278.
(39) Neyerlin, K. C.; Bugosh, G.; Forgie, R.; Liu, Z.; Strasser, P. *J. Electrochem. Soc.* **2009**, *156*, B363–B369.
(40) Schmidt, T. J.; Gasteiger, H. A.; Staeb, G. D.; Urban, P. M.; Kolb, D. M.; Behm, R. J. *J. Electrochem. Soc.* **1998**, *145*, 2354–2358.
(41) Schmidt, T. J.; Gasteiger, H. A. In *Handbook of Fuel Cells-Fundamentals, Technology, and Applications*; Vielstich, W., Lamm, A., Gasteiger, H., Eds.; Wiley: Chichester, 2003; Vol. 2, Chapter 22, p 316.
(42) Koh, S.; Strasser, P. *J. Electrochem. Soc.* **2010**, *157*, B585–591.
(43) Liu, Z.; Koh, S.; Yu, C.; Strasser, P. *J. Electrochem. Soc.* **2007**, *154*, B1192–B1199.
(44) Koh, S.; Strasser, P. *J. Am. Chem. Soc.* **2007**, *129*, 12624–12625.
(45) Reddy, A. K. N.; Rao, B. *Can. J. Chem.* **1969**, *47*, 2693–2698.
(46) Strasser, P. *J. Comb. Chem.* **2008**, *10*, 216–224.
(47) Hagemeyer, A., Strasser, P., Volpe, A. F., Eds. *High-Throughput Screening in Chemical Catalysis - Technologies, Strategies and Applications*; Wiley VCH: Weinheim, 2004.
(48) Strasser, P.; Fan, Q.; Devenney, M.; Weinberg, W. H.; Liu, P.; Norskov, J. K. *J. Phys Chem B* **2003**, *107*, 11013.
(49) Fergie, R.; Neyerlin, K. C.; Bugosh, G.; Liu, Z.; Strasser, P. *Electrochem. Solid-State Lett.* **2010**, *13*, B36–B39.
(50) Asazawa, K.; Yamada, K.; Tanaka, H.; Oka, A.; Taniguchi, M.; Kobayashi, T. *Angew. Chem.* **2007**, *46*, 1–5.
(51) Liu, Z.; Yu, C.; Rusakova, I.; Huang, D.; Strasser, P. *Top. Catal.* **2008**, *49*, 241–250.
(52) Greeley, J.; Norskov, J. K.; Kibler, L. A.; El-Aziz, A. M.; Kolb, D. M. *ChemPhysChem* **2006**, *7*, 1032–1035.
(53) Nørskov, J. K.; Bligaard, T.; Logadottir, A.; Kitchin, J. R.; Chen, J. G.; Pandelov, S.; Stimming, U. *J. Electrochem. Soc.* **2005**, *152*, J23–J26.
(54) Baltruschat, H. *J. Am. Soc. Mass Spectrom.* **2004**, *15*, 1693–1706.
(55) Wang, H.; Loeffler, T.; Baltruschat, H. *J. Appl. Electrochem.* **2001**, *31*, 759–765.
(56) Vayenas, C. G.; Bebelis, S.; Yentekakis, I. V.; Lintz, H. G. *Catal. Today* **1992**, *11*, 303–442.
(57) Baranova, E. A.; Thursfield, A.; Brosda, S.; Foti, G.; Comninellis, C.; Vayenas, C. G. *J. Electrochem. Soc.* **2005**, *152*, E40–E49.
(58) Hammer, B.; Nørskov, J. K. *Surf. Sci.* **1995**, *343*, 211–220.
(59) Bard, A. J.; Faulkner, L. R. *Electrochemical Methods*; Wiley: New York, 1980.
(60) Jiang, Y.; Yentekakis, I. V.; Vayenas, C. G. *Science* **1994**, *264*, 1563.
(61) Lipkowski, J.; Ross, P. N.; Sun, S. G. Studying Electrocatalytic Oxidation of Small Organic Molecules with In-Situ Infrared spectroscopy. In *Electrocatalysis*; Lipkowski, J., Ross, P. N., Eds.; Wiley-VCH: New York, 1998, p 143.
(62) Jarvi, T. D.; Stuve, E. M., Fundamental Aspects of Vacuum and Electrocatalytic Reactions of Methanol and Formic Acid on Platinum Surfaces. In *Electrocatalysis*; Lipkowski, J., Ross, P. N., Eds.; Wiley-VCH: New York, 1998, p 75.
(63) Herrero, E.; Chrzanowski, W.; Wieckowski, A. *J. Phys. Chem.* **1995**, *99*, 10423–10424.
(64) Strasser, P.; Eiswirth, M.; Ertl, G. *J. Chem. Phys.* **1997**, *107*, 991.
(65) Strasser, P.; Luebke, M.; Raspel, F.; Eiswirth, M.; Ertl, G. *J. Chem. Phys.* **1997**, *107*, 979.
(66) Strasser, P.; Eiswirth, M.; Koper, M. T. M. *J. Electroanal. Chem.* **1999**, *478*, 50.